第 44 卷 第 5 期/2024 年 3 月/光学学报 研究论文

光学学报

共程 Tolansky 干涉圆环嵌套现象分析

欧阳烨锋，许子杰，张宝武*，朱玲，方振远，罗贤欢，孙怡

中国计量大学计量测试工程学院，浙江 杭州 310018

摘要 针对共程 Tolansky 干涉测量中出现的干涉圆环嵌套问题，基于多光束反射原理建立了分析模型，通过将 MATLAB 的仿真实验和实体双臂 Tolansky 干涉系统相结合的方式进行交叉验证，结果显示嵌套环确实是由光束在干涉分光镜和干涉反射镜之间来回反射产生的多光束干涉造成的。由仿真和实验的验证显示可知，通过合理调整干涉分光镜的透射率、反射率和干涉反射镜的反射率可以对嵌套现象进行有效地抑制，为后续利用共程 Tolansky 干涉进行精密测量提供了理论和实验指导。

关键词 物理光学；Tolansky 干涉；共程干涉；非定域；圆环嵌套

中图分类号 TP394.1；TH691.9 **文献标志码** A **DOI：** 10.3788/AOS231856

1 引 言

随着人工智能、大数据和云计算等科技的发展，半导体行业成为大国竞争的关键性领域[1-4]。在芯片制造中，晶片厚度及其整体厚度的均匀性、可靠性和稳定性等性能对行业成本的降低及生产和供应链的平稳顺畅来说非常重要[5-8]。目前，超精密厚度加工技术对检测精度的要求越来越高，各种传统测厚方法（如电感测微法、电容法等非干涉非接触法、激光光谱法、超声法、X 射线法）也越来越难以满足该需求，而基于干涉原理的双端面测厚方法因具有高精度特点逐渐成为测厚方法研究热点[9-11]。这种方法使用双路干涉光直接对射厚度样品两个端面，使测量结果只与厚度样品端面特性、测量光路和环境参数相关，排除了传统方法中辅助剂、辐射、厚度样品内部光程等因素影响。例如，日本计量院提出相移式迈克耳孙干涉双端测厚系统，在实验室对量块进行测量，获得的测量重复性优于 3 nm[9]，对晶圆厚度进行测量时，测量扩展不确定度为 20 nm（包含因子 $k=2$）[10]。德国联邦物理技术研究院（PTB）采用相似的系统对量块进行测量，获得的测量重复性优于 2 nm[9]。在双端面测厚方法研究方面，日本[12-14]、德国[15-17]、波兰[18-19]、捷克[20-22]等国家和区域已经取得了非常好的成果。

Tolansky[23-24]干涉可以兼顾角度和厚度测量，为双端面高精度测厚方法的发展提供了一种新的可能。其中，厚度测量是通过 Tolansky 干涉同心圆环的半径来解算，角度测量是通过 Tolansky 干涉同心圆环的圆心侧移量来解算。基于此，提出共程 Tolansky 干涉精密测量技术。实验研究发现，这种技术存在一种干涉圆环嵌套现象。本文基于几何光学原理分析了嵌套现象的原因，以此为基础，利用 MATLAB 对嵌套干涉圆环进行了仿真，并将其与实验干涉图像进行比对。

2 共程 Tolansky 干涉系统

Tolanshy 干涉本质上是一种点光源非定域干涉，干涉原理图如图 1(a)所示。利用系列光学元件将激光会聚后构建出两个相距 d 的点光源 S_1 和 S_2，它们各自发出的球面光波分别经过 r_1 和 r_2 路径后在空间 P 点相遇叠加，点光源 S_1 与 P_0 点之间的距离为 L_0。在 P_0 点垂直于 x 轴的平面内就可以观察到一个同心圆环干涉图形，如图 1(b)所示，其中，干涉圆环的圆心即为 P_0 点，任意一环的半径记为 R_i。

基于图 1 的 Tolansky 干涉原理，搭建了一套共程光学测量系统，如图 2(a)所示。激光光源发出的激光束通过一系列光学元件并在观察分光镜处会聚形成一个点光源，随后依次通过干涉分光镜和干涉反射镜反射原路返回，并在面阵电荷耦合器件（CCD）处形成共程干涉图像，共程干涉图像如图 2(b)所示。其中，干涉分光镜的厚度为 d_1，折射率为 n_1，前表面镀有分光膜，离点光源 S 的距离为 D，后表面镀有增透膜，与干涉反射镜之间的距离为 d_0，其间的折射率为 n_0，CCD 离点光源的距离为 L，其间的折射率为 n_0。这样，点光源 S 经过干涉分光镜前表面形成一个虚点光源 S_1，经

收稿日期：2023-11-29；**修回日期**：2023-12-13；**录用日期**：2023-12-29；**网络首发日期**：2024-01-09

基金项目：国家市场监督察理总局科技计划项目资助(2022MK220)、中国计量大学校教改课题(HEX2023005)

通信作者：*zhangbaowu@126.com

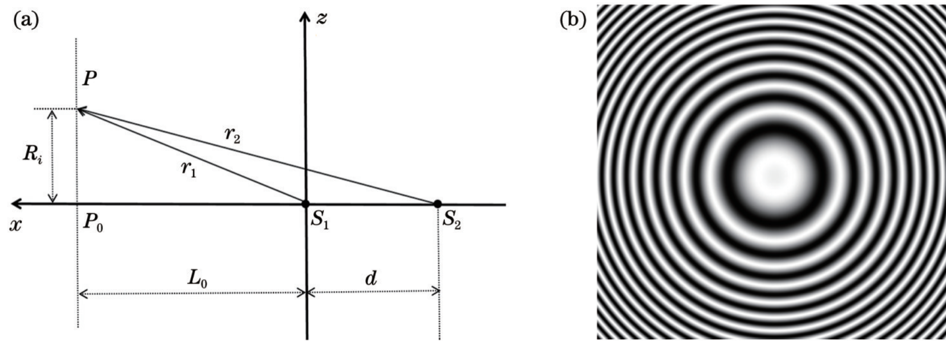

图1 Tolansky干涉原理。(a)原理光路;(b)干涉同心圆环

Fig. 1 Principle of Tolansky interference. (a) Principle optical path; (b) interference concentric rings

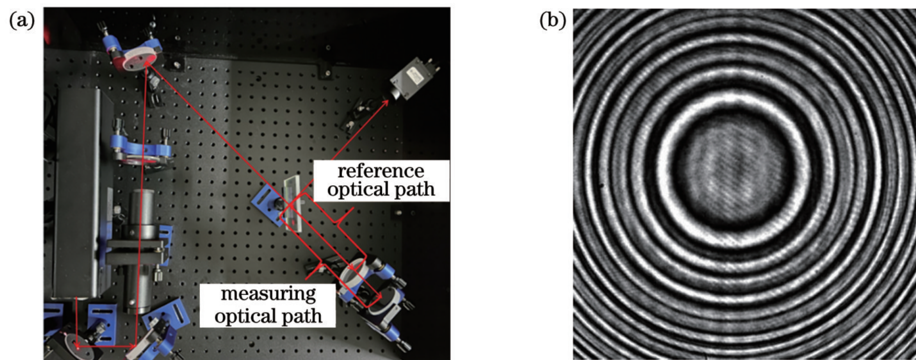

图2 共程干涉仪器及实验结果。(a)共程干涉光路;(b)共程干涉光路结果

Fig. 2 Common-path interference instrument and experimental results. (a) Common-path interference optical path; (b) result of common-path interference optical path

过干涉反射镜形成虚点光源S_2,在两者叠加照亮的区域处可以产生非定域干涉,如图3所示。

实验发现,图2(b)的干涉同心圆环存在明显的嵌套环现象,与图1(b)单圆环结构不同。这种现象会使干涉图像的圆心和半径识别产生误差,进而影响厚度和角度测量的精度。

在图2(a)共程Tolansky光路结构基础上,将测量光路和参考光路分离,形成类似迈克耳孙干涉仪的双臂光路结构,如图4(a)所示。其中光线的路径示意由箭头标注。与图2(a)相比,图4(a)用一个反射镜代替干涉分光镜,与原来的干涉反射镜形成空气型Tolansky干涉结构,不再出现多次来回反射的问题,

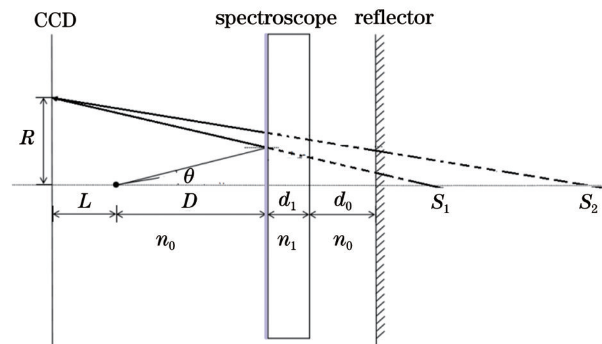

图3 干涉示意图

Fig. 3 Interference diagram

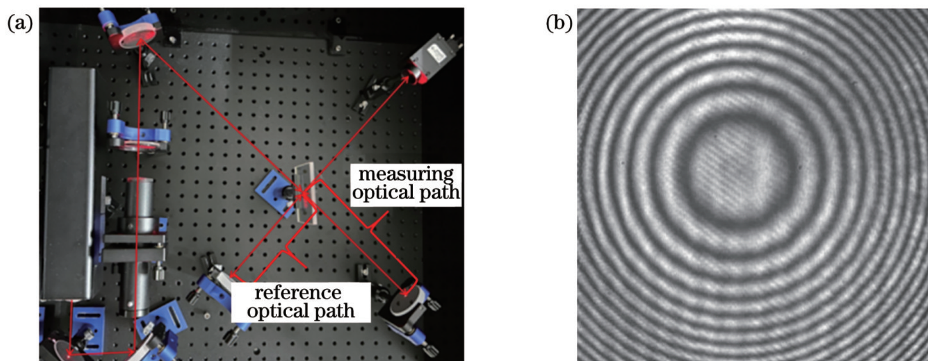

图4 双臂光路Tolansky干涉系统。(a)系统布局;(b)干涉同心圆环

Fig. 4 Dual-arm optical path Tolansky interference system. (a) System layout; (b) interference concentric rings

此时形成的干涉图像如图 4(b)所示。与图 2(b)相比，图 4(b)的双臂光路干涉图形确实不存在明显的嵌套现象。这可以说明嵌套现象的确来自于光学在各镜面间的来回反射。

3 嵌套现象分析

3.1 理论分析

研究发现，图 2 显示的嵌套现象来源于干涉分光镜和干涉反射镜之间的多次来回反射，如图 5 所示。

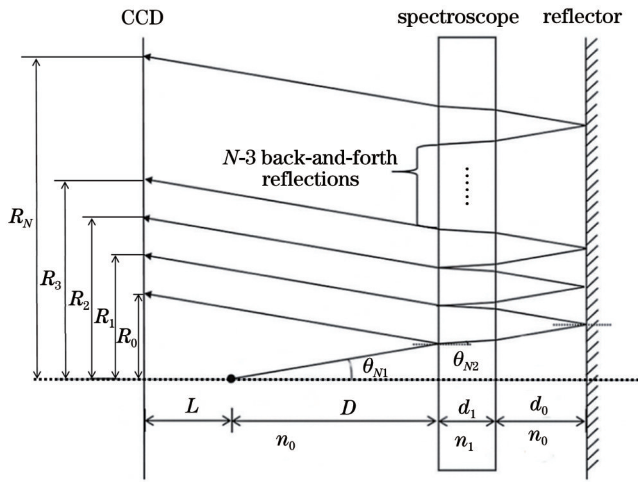

图 5 来回反射示意图

Fig. 5 Diagram of back-and-forth reflection

当点光源 S 所发出的任一以 θ_{N1} 角入射的光线(波长为 λ)在干涉分光镜和干涉反射镜之间来回反射 N 次($N\geqslant1$)后抵达面阵 CCD 上距离光轴 R_N 的点时，根据光程的计算方式，即光程等于光在介质中通过的几何路径与该介质折射率的乘积，得到光线走过的光程为

$$\Delta_N=\frac{L+2D+2Nd}{\cos\theta_{N1}}n_0+\frac{2d_1}{\cos\theta_{N2}}n_1+\frac{1}{2}N\lambda,\tag{1}$$

其中

$$\cos\theta_{N1}=\frac{L+2D+2Nd+2Nd_1n_0/n_1}{\sqrt{\left(L+2D+2Nd+2Nd_1n_0/n_1\right)^2+R_N^2}},\tag{2}$$

$$\cos\theta_{N2}=\sqrt{1-\left[\frac{R}{\sqrt{\left(L+2D+2Nd+2Nd_1n_0/n_1\right)^2+R_N^2}}\frac{n_0}{n_1}\right]^2}。\tag{3}$$

当来回反射次数为 1 时，即 $N=1$ 时，式(1)为简单的双光束干涉。

物理光学知识指出，平行出射的光线在有限距离处并不会产生干涉现象，但它们会和其他以不同的入射角入射的光线经过不同的来回反射 N 次后抵达距离光轴 R 的点的光发生干涉现象，其干涉过程如图 6(a)所示。

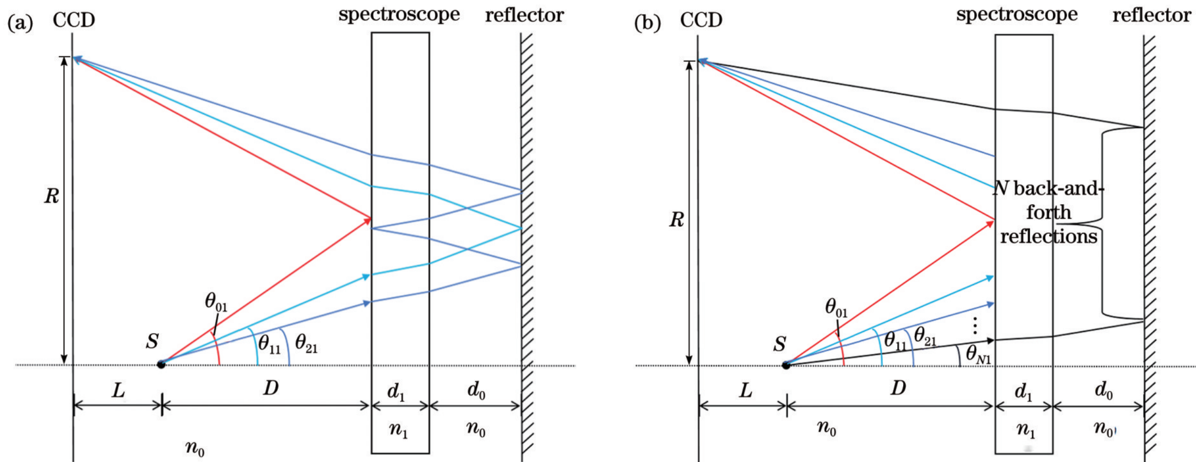

图 6 多光束干涉示意图。(a)前三次来回反射产生干涉；(b)前 N 次来回反射产生干涉

Fig. 6 Schematic diagram of multi-beam interference. (a) Interference from the first three back-and-forth reflection; (b) interference from the first N back-and-forth reflection

在图 6(a)中，光线 1、2、3 分别以 θ_{01}、θ_{11}、θ_{21} 的角度进入光学系统，经过干涉分光镜和干涉反射镜来回反射作用了 0、1、2 次，最终在 CCD 上的距离光轴为 R 的点处相遇，产生干涉。由此可以进行递推，如图 6(b)所示，经分光镜和反射镜来回反射 N 次的光线也抵达了距离光轴为 R 的点，那么这条光线的入射角 θ_{N1} 可以由式(2)计算得到，而光线抵达距离光轴 R 的点时的光程可以由式(1)计算得到。这样，$N+1$ 条光线在距离光轴 R 的点相遇产生干涉后的干涉光强为

$$I_R=\sum_{i=0}^{N-1}\sum_{j=i+1}^{N}\left[I_i+I_j+2\sqrt{I_iI_j}\cos\left(2\pi\frac{\Delta_i-\Delta_j}{\lambda}\right)\right],\tag{4}$$

式中：Δ_i 和 Δ_j 分别为第 i 束和第 j 束光抵达 CCD 时的光程。

经过来回反射 N 次的光线光强受到干涉分光镜的透射率 K_t 和反射率 K_r、反射镜的反射率 K 影

响，光源的出射光强为I，则来回反射N次的光线光强为

$$I_N = IK_t^2 K_r^N K^{N+1}。\tag{5}$$

3.2 仿真分析

基于式(4)，利用表1所示的MATLAB参数进行可视化仿真，进一步研究嵌套环现象。

表1 MATLAB仿真所用参数

Table 1 Parameters used in MATLAB simulation

Dimension parameter	Value	Physical parameter	Value
Distance between CCD and light source /mm	915.0	Illuminance of light source /lx	80
Distance between light source and spectroscope /mm	84.0	Optical maser wavelength /nm	532
Distance between splitter and reflector /mm	49.9	Refractive index of air	1.0003
Thickness of spectroscope /mm	1.0	Refractive index of spectroscope	1.4611

不考虑分光镜和反射镜间的来回反射，即N=1时，干涉系统就是简单的双光束干涉，此时的干涉图像如图7所示。其中，图7(a)为二维干涉同心圆环结构，图7(b)为干涉图像过圆心沿直径方向的光强变化曲线。图7(b)显示的干涉同心圆环图像从圆心往外的强度分布并非标准的正余弦波形，离圆心中心越远，波形周期越小。因此图7(a)表现为亮暗分布的圆环且由圆心往外圆环迅速变得密集。

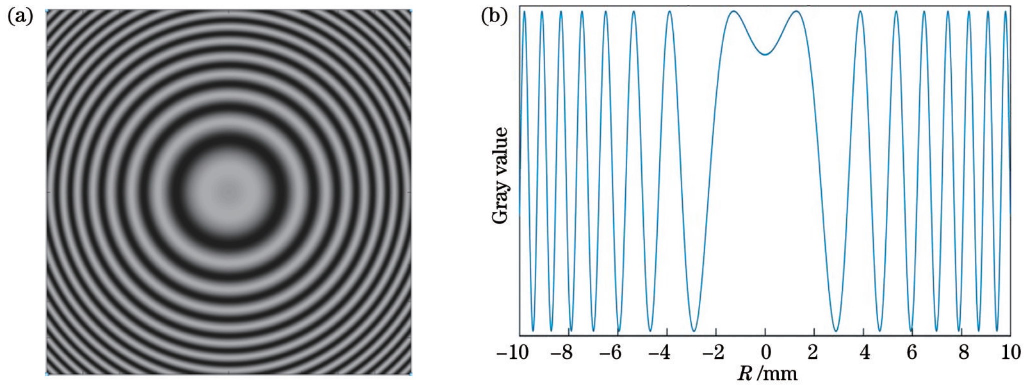

图7 仿真结果。(a)仿真干涉图；(b)亮度变化曲线

Fig. 7 Simulation result. (a) Simulated interferogram; (b) brightness variation curve

当光线来回反射次数大于1时，由式(4)可知，干涉系统在N>1时为多光束干涉，这一结果也更加贴近真实的实验结果。以表1给出的各物理参量为基础，取N=3，在不同总光强I、干涉分光镜透射率K_t和反射率K_r，以及干涉反射镜反射率K情况下进行仿真，得到结果如图8所示。如表2所示，考虑现实条件约束，参数均选用实验室中常见的分光镜参数。

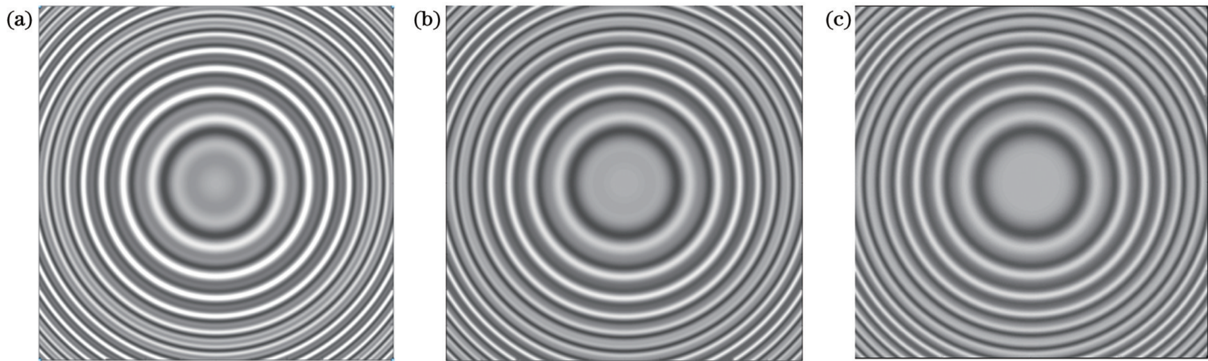

图8 N=3时不同透射、反射率下的干涉结果。(a)组1；(b)组2；(c)组3

Fig. 8 Interference results under different transmittance and reflectivity for N=3. (a) Group 1; (b) group 2; (c) group 3

从图8中可以看出，首先，各光学镜面间的来回反射导致的多光束干涉模型，其干涉图像确实存在嵌套现象，这与上文所给出的理论相互吻合。其次，随着干涉分光镜透射率K_t、反射率K_r、干涉反射镜反射率K的调整，光强I_N随着来回反射次数N的增大而减弱，嵌套的现象也有明显减弱。为了进一步证明调整透

表 2　各仿真图像对应参数

Table 2　Corresponding parameters of simulation image

Group	Light intensity I /cd	Spectroscope transmittance K_t	Spectroscope reflectance K_r	Reflector reflectance K
1	20	0.5	0.5	1.0
2	50	0.7	0.3	0.5
3	80	0.8	0.2	0.3

射率、反射率对嵌套现象的影响，选择具有代表性的图 8(a)和图 8(c)结果分别以圆心为轴线绘制光强变化曲线，并与图 7(b)进行比较，其对比结果如图 9所示。

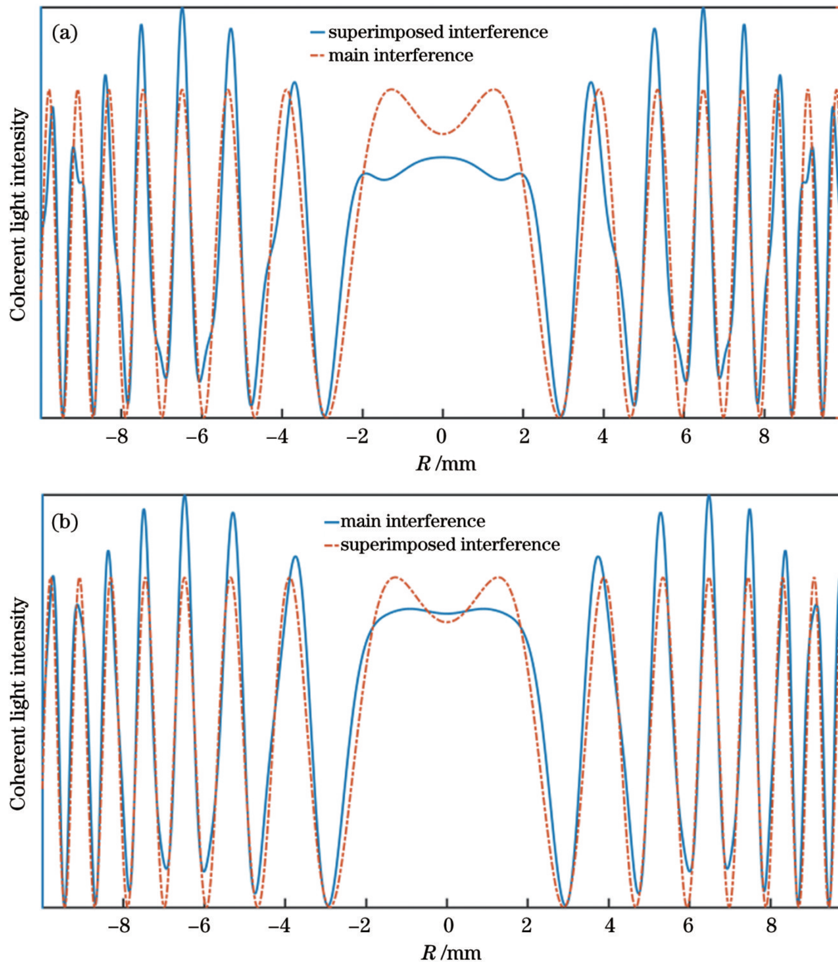

图 9　不同透射率、反射率下的干涉图像灰度变化曲线。(a)图 8(a)对比结果；(b)图 8(c)对比结果

Fig. 9　Gray-scale variation curves of interference images under different transmittance and reflectivity. (a) Fig. 8(a) comparison result; (b) Fig. 8(c) comparison result

在图 9(a)中，实线对应强嵌套圆环亮暗分布情况，虚线对应双光束干涉结果，即图 8(b)。从二者对比图可以看出，多光束干涉结果的各个主要波形都会附带一个明显的叉分波形，这些叉分波形在干涉图形上所呈现的视觉效果就是嵌套环。而在干涉中心区域，其亮暗分布甚至与主干涉的相反，即图像中心的暗斑反而成了一个亮斑，这会使圆心干涉级次的判断产生误差，影响厚度测量。

从图 9(b)可以看出，减小干涉分光镜和干涉反射镜的反射率，可以使它们之间来回反射光束的光强迅速减弱，使干涉图像更加近似于双光束干涉结果，且两条波形曲线的各峰值、谷值基本在同一位置，每一个圆环对应的波形上没有明显的分叉，可以有效地减小嵌套环带来的影响。

3.3　实验验证

此外，为了进一步验证干涉分光镜透射率 K_t、反射率 K_r、干涉反射镜反射率 K 这三个参数对干涉中来回反射光路的抑制效果，给出如图 10 所示的光路结构图。通过更换图 10 结构中 mirror 1 和 mirror 2 两块光学透镜便可采集不同反射率、透射率下的干涉图像，进一步分析并验证嵌环套现象减弱这一效果。

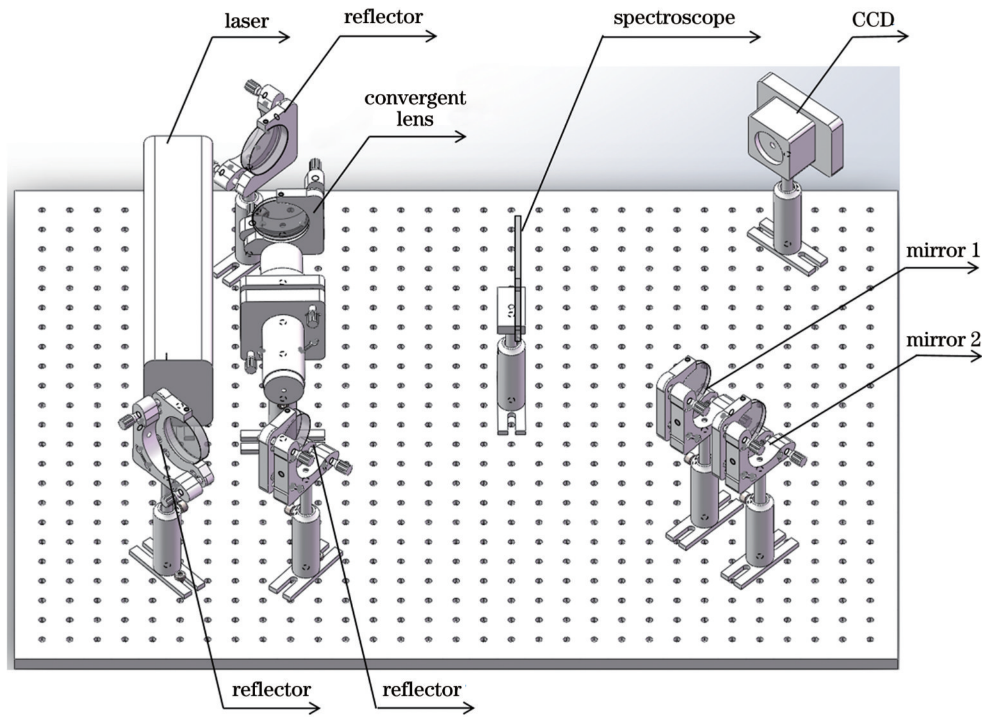

图 10　共程 Tolansky 干涉系统

Fig. 10　Common-path Tolansky interference system

与图 2(a)相比，图 10 的 mirror 1 和 mirror 2 分别采用不同反射率、透射率的分光镜，实验所采集到的图像如图 11 所示，其 3 幅不同干涉图像所对应的具体 K_t、K_r、K 值和上文仿真所设值保持一致，具体数据见表 2。由图 11 可知，随着两个反射率 K_r、K 的降低，嵌套现象有明显的减弱。需要指出的是，在实际镀膜过程中，工艺、原料等因素所带来的误差在 ±1% 之内，经过仿真分析，这一误差仅使得干涉图片在亮度上有细微变化，但对亮暗强度分布没有明显影响。

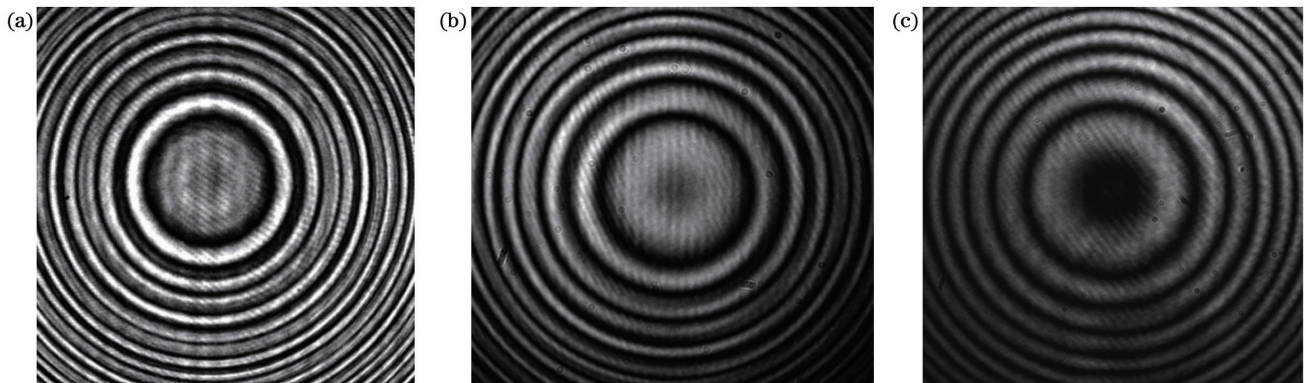

图 11　不同透射率、反射率下的实验结果。(a)组 1；(b)组 2；(c)组 3

Fig. 11　Interference results under different transmittance and reflectivity. (a) Group 1; (b) group 2; (c) group 3

4　结　　论

基于多光束干涉原理提出共程 Tolansky 嵌套干涉圆环理论，嵌套干涉现象来自干涉分光镜与干涉反射镜之间的来回反射。这使每个干涉圆环上的波形出现分叉，使圆心处的干涉级次发生变化，导致每个圆环的半径和圆心识别产生误差，从而影响对应干涉级次的确定，不利于基于 Tolansky 干涉的精密测量。同时，MATLAB 仿真和实验结果表明，在共程 Tolansky 干涉系统中可以通过调整干涉分光镜的透射率、反射率和干涉反射镜的反射率来抑制嵌套现象，使经过来回反射的光束强度迅速减弱，从而使干涉结果近似为双光束干涉，为后续利用共程 Tolansky 干涉进行精密测量提供指导。

参　考　文　献

[1] Zhang M S. Research on high precision of projection exposure imaging of large-scale integrated circuit lithography machine[J]. Journal of Physics: Conference Series, 2021, 1952(2): 022020.

[2] 付鹏，张艳春，赵涛，等. 高效率高功率976 nm半导体激光芯片设计与制备[J/OL]. 中国激光: 1-13[2023-11-15]. https://kns.cnki.net/kcms/detail/31.1339.tn.20231114.1001.002.html.
Fu P, Zhang Y C, Zhao T, et al. Design and fabrication of high-efficiency and high-power 976 nm semiconductor laser chips [J/OL]. Chinese Journal of Lasers: 1-13[2023-11-15]. https://kns.cnki.net/kcms/detail/31.1339.tn.20231114.1001.002.html.

[3] Wang S X, Kong L B, Wang C J, et al. Ultra-precision manufacturing of microlens arrays using an optimum machining process chain[J]. Optics Express, 2023, 31(2): 2234-2247.

[4] 张云山，赵同飞，施建琴，等. 单片集成两段式双波长分布反馈半导体激光器[J]. 光学学报, 2023, 43(10): 1014002.
Zhang Y S, Zhao T F, Shi J Q, et al. Monolithic integrated two-section dual-wavelength distributed feedback semiconductor laser[J]. Acta Optica Sinica, 2023, 43(10): 1014002.

[5] 李隆，杨建花，张春玲，等. 脉冲LD端面泵浦YAG/Nd:YAG复合晶体热效应分析[J]. 激光与光电子学进展, 2022, 59(21): 2114001.
Li L, Yang J H, Zhang C L, et al. Thermal effect analysis of pulsed LD end-pumped YAG/Nd: YAG composite crystal[J]. Laser & Optoelectronics Progress, 2022, 59(21): 2114001.

[6] 王秀秀. 基于激光位移传感器的晶圆检测调焦技术研究[D]. 桂林: 桂林电子科技大学, 2022.
Wang X X. Research on laser displacement sensor based wafer inspection and focusing technology[D]. Guilin: Guilin University of Electronic Technology, 2022.

[7] den Boef A J. Optical wafer metrology sensors for process-robust CD and overlay control in semiconductor device manufacturing[J]. Surface Topography: Metrology and Properties, 2016, 4(2): 023001.

[8] 冯明春，刘文清，徐亮，等. 迈克耳孙干涉仪中的镜面面形误差研究分析[J]. 光学学报, 2015, 35(4): 0423002.
Feng M C, Liu W Q, Xu L, et al. Analysis of the mirror surface errors in a Michelson interferometer[J]. Acta Optica Sinica, 2015, 35(4): 0423002.

[9] 湛敏. 一种双端面非接触双分光式迈克尔逊干涉测厚方法: CN115371573A[P]. 2022-11-22.
Zhan M. The invention relates to a double-end non-contact double-split Michelson interference thickness measurement method: CN115371573A[P]. 2022-11-22.

[10] Hirai A, Bitou Y, Bae J, et al. Precise measurement of the thickness of silicon wafers by double-sided interferometer and bilateral comparison[J]. Metrologia, 2021, 58(5): 054002.

[11] 张宝武，孔明，沈超，等. 一种量块双端面无研合自溯源光学干涉测量方法: CN114993189A[P]. 2022-09-02.
Zhang B W, Kong M, Shen C, et al. A non-research self-traceable optical interferometry method for measuring block double end faces is presented: CN114993189A[P]. 2022-09-02.

[12] Ishii Y, Seino S. New method for interferometric measurement of gauge blocks without wringing onto a platen[J]. Metrologia, 1998, 35: 67-73.

[13] Kuriyama Y, Yokoyama Y, Ishii Y, et al. Development of a new interferometric measurement system for determining the main characteristics of gauge blocks[J]. CIRP Annals, 2006, 55 (1): 563-566.

[14] Agustinus W, Hirai A, Takahashi S, et al. Novel measurement technique of gauge block without wringing using a tandem low-coherence interferometer[EB/OL]. [2023-11-09]. http://www.nanolab.t.u-tokyo.ac.jp/pdffiles/3I08-ASPEN1A2-5-1807.pdf.

[15] Abdelaty A, Walkov A, Franke P, et al. Challenges on double ended gauge block interferometry unveiled by the study of a prototype at PTB[J]. Metrologia, 2012, 49(3): 307-314.

[16] Rau K, Schödel R. Double-ended interferometer for measuring gauge blocks without wringing[M]//Osten W. Fringe 2013. Heidelberg: Springer, 2014: 859-862.

[17] Fischedick M, Stavridis M, Bartl G, et al. Investigation of the uncertainty contributions of the alignment of PTB's double-ended interferometer by virtual experiments[J]. Metrologia, 2021, 58(6): 064001.

[18] Dobosz M, Iwasinska-Kowalska O. A new method of non-contact gauge block calibration using a fringe-counting technique: I. Theoretical basis[J]. Optics & Laser Technology, 2010, 42 (1): 141-148.

[19] Iwasinska-Kowalska O, Dobosz M. A new method of noncontact gauge block calibration using the fringe counting technique: II. Experimental verification[J]. Optics & Laser Technology, 2010, 42(1): 149-155.

[20] Buchta Z, Řeřucha S, Mikel B, et al. Novel principle of contactless gauge block calibration[J]. Sensors, 2012, 12(3): 3350-3358.

[21] Buchta Z, Řeřucha Š, Mikel B, et al. System for contactless gauge blocks measurement[J]. Proceedings of SPIE, 2013, 8759: 875915.

[22] Buchta Z, Šarbort M, Čížek M, et al. System for automatic gauge block length measurement optimized for secondary length metrology[J]. Precision Engineering, 2017, 49: 322-331.

[23] Tolansky S. LXIV. New contributions to interferometry. Part I: new non-localized interference fringes[J]. The London, Edinburgh, and Dublin Philosophical Magazine and Journal of Science, 1943, 34(235): 555-565.

[24] Wang Y C, Shyu L H, Chang C P. Fabry-Pérot interferometer utilized for displacement measurement in a large measuring range[J]. Review of Scientific Instruments, 2010, 81(9): 093102.

Ring Nesting Phenomenon Analysis in Common-Path Tolansky Interference

Ouyang Yefeng, Xu Zijie, Zhang Baowu*, Zhu Ling, Fang Zhenyuan, Luo Xianhuan, Sun Yi

College of Metrology and Measurement Engineering, China Jiliang University, Hangzhou 310018, *Zhejiang, China*

Abstract

Objective The thickness measurement method based on dual-channel light directly radiating on the two end faces of the thickness sample has gradually become an international hotspot. This is because the measurement results are only related to the end face characteristics of the thickness sample, the measurement optical path and environmental parameters, and the influence of the auxiliary agent, radiation, with the internal optical path of the thickness sample in the traditional method

excluded. Among these, Tolansky interferometry features both angle and thickness measurements, which provides a new possibility for research into high-precision thickness measurement methods for double-end faces. Additionally, this means that the series radius of the interference concentric ring is adopted to calculate the measured thickness. In the thickness measurement using the common-path Tolansky interference scheme, the image of the interference concentric ring has an obvious ring nesting phenomenon, and even misaligned nesting occurs. This phenomenon will affect the image recognition accuracy of the radius and interfere with the subsequent thickness measurement results. Therefore, it is important to investigate technical schemes to eliminate or suppress this phenomenon in thickness measurements using the common-path Tolansky interference scheme.

Methods Based on the dual-beam interference principle of the point light source, the Tolansky interference image is displayed by MATLAB virtual simulations. Then the experimental pictures of whether the interference concentric rings are different or not are displayed via the common-path Tolansky interferometer and the dual-arm optical path structure experimental system similar to the Michelson interferometer. That means there is an interference loop nesting in the former, and no interference loop nesting in the latter. After a detailed study, it is found that the biggest difference between the two systems is the existence of a multi-faceted structure of the common-path Tolansky. Additionally, the laser will reflect multiple times between these faces, while the dual-arm optical path structure similar to the Michelson interferometer does not have this multiple reflection phenomenon.

Given this, based on the geometrical optics principle, we employ the multiple reflection method to carry out theoretical analysis and formula derivation and obtain the expression of optical path difference and interference intensity different from double beam interference. Meanwhile, the correlation relationship between the beam intensity after multiple reflections and the incident light intensity of the interference spectrometer, the transmittance K_t, the reflectivity K_r, and the reflectivity K of the mirror is acquired. Thus, a new simulation model of interference concentric rings is obtained. On this basis, the interference concentric ring is simulated by MATLAB. The simulation results show that the interference concentric rings obtained based on the multiple reflection theory are in good agreement with the experimental images in terms of the structure and intensity profile, which also confirms the correctness of the theory. Given the strong correlation between the beam intensity after multiple reflections and the parameters of incident light intensity, transmittance K_t, reflectivity K_r, and reflectivity K, the interference concentric ring images with different collocations of these parameters are further virtually studied. The results show that by adjusting the transmittance and reflectivity of the interferometric spectroscope and the reflectivity of the interferometric mirror, the nesting phenomenon can be suppressed.

Based on the theoretical analysis and virtual simulation, interference spectrometers with different spectral ratios and interference mirrors with different reflectivities are replaced in the common-path Tolansky interference experimental system to realize different collocations among these parameters. The experimental results are in good agreement with the virtual simulation results, which verify the proposed method for suppressing the nesting phenomenon.

Results and Discussions We propose an analysis method of multiple reflections among multiple planes, and obtain the expression of optical path difference and interference intensity different from double beam interference. Meanwhile, the correlation between the beam intensity after multiple reflections and the incident light intensity of the interference spectrometer, transmittance K_t, reflectivity K_r, and reflectivity K of the reflector is obtained. Thus, a new simulation model of an interference concentric ring is obtained, with the theory of common-path Tolansky interference analysis perfected.

Based on a new theoretical basis, a method to suppress the nesting phenomenon of the interference ring is proposed to suppress the phenomenon by reasonably adjusting the transmittance, reflectance of the interference spectrometer, and reflectivity of the interference mirror. Finally, a guarantee is provided for accurate extraction of the series ring radius by the common-path Tolansky interference thickness measurement technology.

Conclusions The nesting or misplaced nesting of the common-path Tolansky interference ring causes bifurcation and ambiguity in each interference ring, which not only changes the interference level at the center of the circle, but also affects the recognition accuracy of each ring radius. As a result, there will be errors in the measured thickness inversion via the ring radius, which is unfavorable for accurate thickness measurement using the common-path Tolansky interference. The MATLAB virtual simulation and experimental results show that the nesting phenomenon comes from multiple reflections among multiple surfaces, and the intensity of the reflected light beam can be quickly weakened by adjusting the transmittance and reflectance of the interference spectroscope and the reflectivity of the interference mirror reasonably. Finally, the interference result is approximately double beam interference, and the nesting phenomenon is effectively restrained. This provides a guarantee for accurate radius extraction of the common-path Tolansky interference concentric ring series and accurate thickness measurements.

Key words physical optics; Tolansky interference; common-path interference; non-localized; ring nesting